

Transcriptomic characterization of human choroidal neovascular membranes identifies calprotectin as a novel biomarker for patients with age-related macular degeneration

Anja Schlecht, Stefaniya Boneva, Markus Gruber, Peipei Zhang, Ralf Horres, Felicitas Bucher, Claudia Auw-Haedrich, Lutz Hansen, Andreas Stahl, Ingo Hilgendorf, Hansjürgen Agostini, Peter Wieghofer, Günther Schlunck, Julian Wolf, Clemens A.K. Lange

Angaben zur Veröffentlichung / Publication details:

Schlecht, Anja, Stefaniya Boneva, Markus Gruber, Peipei Zhang, Ralf Horres, Felicitas Bucher, Claudia Auw-Haedrich, et al. 2020. "Transcriptomic characterization of human choroidal neovascular membranes identifies calprotectin as a novel biomarker for patients with age-related macular degeneration." *The American Journal of Pathology* 190 (8): 1632-42.
<https://doi.org/10.1016/j.ajpath.2020.04.004>.



BIOMARKERS, GENOMICS, PROTEOMICS, AND GENE REGULATION

Transcriptomic Characterization of Human Choroidal Neovascular Membranes Identifies Calprotectin as a Novel Biomarker for Patients with Age-Related Macular Degeneration



Anja Schlecht,* Stefaniya Boneva,* Markus Gruber,* Peipei Zhang,* Ralf Horres,[†] Felicitas Bucher,* Claudia Auw-Haedrich,* Lutz Hansen,* Andreas Stahl,*[‡] Ingo Hilgendorf,[§] Hansjürgen Agostini,* Peter Wieghofer,[¶] Günther Schlunck,* Julian Wolf,* and Clemens A.K. Lange*

From the Eye Center,* Medical Center, Faculty of Medicine, and the Heart Center Freiburg,[§] University of Freiburg, Freiburg; the GenXPro GmbH,[†] Frankfurt Innovation Center Biotechnology, Frankfurt; the Department of Ophthalmology,[‡] University Medical Center Greifswald, Greifswald; and the Institute of Anatomy,[¶] Leipzig University, Leipzig, Germany

Accepted for publication
April 8, 2020.

Address correspondence to
Clemens A.K. Lange, M.D.,
Ph.D., Eye Center, Medical
Center—University of Freiburg,
Killianstrasse 5, Freiburg
79106, Germany. E-mail:
clemens.lange@uniklinik-freiburg.de.

Recent studies deciphering the transcriptional profile of choroidal neovascularization (CNV) in body donor eyes with neovascular age-related macular degeneration are limited by the time span from death to preservation and the associated 5'-RNA degradation. This study therefore used CNV and control specimens that were formalin-fixed and paraffin-embedded immediately after surgical extraction and analyzed them by a 3'-RNA sequencing approach. Transcriptome profiles were analyzed to estimate content of immune and stromal cells and to define disease-associated gene signatures by using statistical and bioinformatics methods. This study identified 158 differentially expressed genes (DEGs) that were significantly increased in CNV compared with control tissue. Cell type enrichment analysis revealed a diverse cellular landscape with an enrichment of endothelial cells, macrophages, T cells, and natural killer T cells in the CNV. Gene ontology enrichment analysis found that DEGs contributed to blood vessel development, extracellular structure organization, response to wounding, and several immune-related terms. The S100 calcium-binding proteins A8 (S100A8) and A9 (S100A9) emerged among the top DEGs, as confirmed by immunohistochemistry on CNV tissue and protein analysis of vitreous samples. This study provides a high-resolution RNA-sequencing-based transcriptional signature of human CNV, characterizes its compositional pattern of immune and stromal cells, and reveals S100A8/A9 to be a novel biomarker and promising target for therapeutics and diagnostics directed at age-related macular degeneration. (*Am J Pathol* 2020, 190: 1632–1642; <https://doi.org/10.1016/j.ajpath.2020.04.004>)

Choroidal neovascularization (CNV) is a common cause of irreversible vision loss in patients with age-related macular degeneration (AMD), which is the leading cause of blindness in the elderly, affecting approximately 200 million individuals worldwide.¹ The introduction of antiangiogenic therapy has enabled significant advances in the treatment of neovascular AMD (nAMD). However, the treatment's success is hampered by the relatively short half-life of antibodies in the eye and depends on frequently repeated intraocular injections that pose a significant cumulative risk of local complications. Approximately one-third of patients with

nAMD lose vision despite continuous anti-vascular endothelial growth factor therapy,² highlighting the complexity of this disease and indicating a relevance of other disease-associated molecular mediators.

Supported by DFG SFB/TRR167 (C.A.K.L.) and Helmut Ecker Foundation grant 02/19 (C.A.K.L.).

J.W. and C.A.K.L. contributed equally as senior authors.

A.S. and S.B. contributed equally to this work.

Disclosures: None declared.

Although genome-wide association studies, animal models, and cell culture systems have provided important insights into nAMD pathogenesis, the underlying cellular and molecular mechanisms in the cascade of events leading to CNV have not been identified in detail. Risk factors for nAMD include increasing age, environmental factors such as smoking, and dietary habits, as well as mutations in susceptibility genes, which predispose an individual to developing AMD. Most AMD gene-association studies published thus far are genome-wide association studies investigating single nucleotide polymorphisms or noncoding single nucleotide polymorphisms associated with CNV formation. These studies have identified several risk factors, such as polymorphisms in the CFH, ARMS2, or C3 genes,³ but they do not provide a detailed view on the biological pathways underlying CNV formation. Gene expression studies on human CNV membranes are therefore becoming increasingly important to move beyond genetic association and comprehensively uncover CNV-associated pathways.⁴

To that end, numerous studies have used microarray technology to explore the expression profiles of normal human eye tissues^{5,6} and to determine genes differentially expressed in eyes of patients with nAMD.⁷ Those studies, however, were limited by their dependence on the standard genome annotations required for probe design and possible cross-hybridization problems.⁸ The more recent availability of RNA-sequencing (RNA-Seq) techniques improved examination of the transcriptome of healthy and diseased tissues, enabling a more accurate and unbiased measurement of gene expression abundance. Moreover, RNA-Seq can assess novel and particularly rare transcripts that have been overlooked by conventional microarray technology so far, and it is also more reproducible due to less technical variation and fewer false-positive findings.^{9,10} All previously published microarray and RNA-Seq studies on CNV membranes, however, are limited by the fact that they have been performed on human donor eyes.^{7,11–14} Because the postmortem interval and the time from death to conservation may range from at best 1 hour to well over 24 hours,¹⁵ it can be assumed that the RNA is already partially degraded. This scenario is particularly critical given the short half-life of mRNA, which ranges between 10 and 25 minutes.¹⁶ Although retinal tissue can provide stable RNA, if processed within 5 hours after death, the retinal pigment epithelium (RPE), which is one of the tissues primarily affected in AMD, must be processed immediately to prevent its decay.¹⁷ To overcome this limitation, the current study analyzed CNV membranes that had been formalin-fixed and paraffin-embedded (FFPE) immediately after surgical extraction from patients with nAMD. Because RNA degradation in FFPE samples is subjected to chemical degradation, which occurs from 5' to 3' ends,¹⁸ a 3'-end RNA sequencing approach called Massive Analysis of cDNA Ends (MACE) was used. This approach allows deciphering of expression signatures, assessment of differential expression,¹⁹ and estimation of the compositional patterns of immune and stromal cells in CNV using the computational method xCell.²⁰

Materials and Methods

Study Population

This study included 11 patients with nAMD and 18 control patients. For RNA-Seq analysis of human CNV membranes, we retrospectively analyzed four consecutive patients with nAMD who underwent subretinal CNV extraction during vitreoretinal surgery between 1992 and 1999. All CNV membranes were treatment-naïve classic CNV and were processed for formalin fixation and paraffin embedding immediately following extraction. Four age-matched FFPE RPE/choroidal specimens obtained in the same period from the macular region of enucleated eyes with ciliary body melanoma served as control samples (Figure 1). For immunohistochemical analysis, the aforementioned FFPE CNV membranes and three randomly chosen and macroscopically normal eyes of three body donors admitted to the Institute of Anatomy were analyzed. Eyes were enucleated in consent with the body donors and secured by contract; no data other than age, sex, weight, and cause of death were disclosed. For protein quantification, seven consecutive patients with nAMD and 11 patients without AMD who underwent vitrectomy for subretinal bleeding or macular pucker between 2017 and 2019 were enrolled. Patients with vitreous hemorrhage, history of previous vitreoretinal surgeries, intraocular inflammations, or concomitant vitreoretinal diseases were excluded. Ethics approval was granted from the Ethics committee of the University of Freiburg, and written informed consent was obtained from each patient.

Sample Collection and Preparation

CNV membranes for RNA-Seq were obtained from four patients by using the currently obsolete technique of subretinal CNV extraction.²¹ Following a 20-gauge vitrectomy, retinotomy was performed temporal to the macula, and the CNV membrane was surgically extracted by using a flexed forceps. The diagnosis was made after a thorough fundoscopic examination of both eyes. Only patients exhibiting a CNV associated with AMD changes, such as drusen and RPE alterations, were included in the study. CNV membranes from patients with other diseases (eg, myopia, history of central serous chorioretinopathy) were not included in this study. Control RPE/choroid samples for RNA-Seq were obtained from the macula region of four enucleated eyes with ciliary body melanoma.

For protein analysis, undiluted vitreous samples (0.5 to 0.8 mL) were obtained from the mid-vitreous of 7 patients with nAMD and 11 patients with epiretinal membrane (control) undergoing vitrectomy using a vitreous cutter at the start of a vitrectomy, before intraocular infusion of fluid. Plasma samples (2 mL) were collected by venous puncture from the same patients after surgery. The vitreous and plasma samples were transferred directly into sterile plastic tubes on ice. The samples were aliquoted and stored at -80°C until analysis.

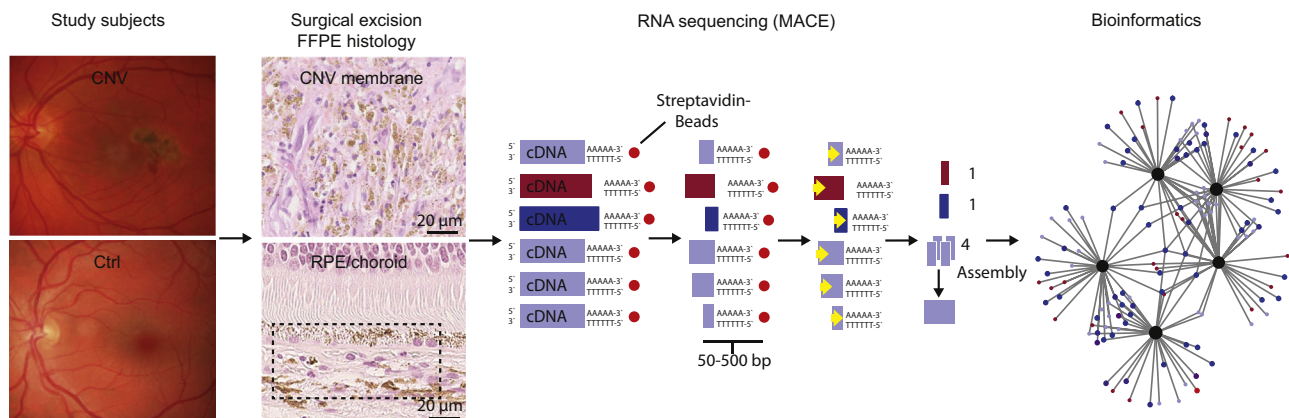


Figure 1 Study subjects and experimental setup for the transcriptional analysis of human choroidal neovascularization (CNV) membranes and control samples. Study subjects were diagnosed after a thorough funduscopy examination. Following surgical CNV excision, the tissue was formalin-fixed and paraffin-embedded (FFPE) before histologic analysis was performed. RNA sequencing was conducted on CNV membranes and healthy retinal pigment epithelium (RPE)/choroid tissue samples (control [Ctrl]) obtained from enucleated eyes (boxed area) using the Massive Analysis of cDNA Ends (MACE) technology. Different colors represent transcripts of different genes, and the respective data were bioinformatically analyzed. Scale bars = 20 µm.

Paraffin Embedding

Formalin fixation and paraffin embedding of CNV membranes and control RPE/choroidal tissue was performed immediately after surgery according to routine protocols, as previously described.¹⁹ Briefly, specimens were fixed immediately after surgery in 4% formalin for 12 hours, dehydrated in alcohol, and finally processed for paraffin embedding. Sections were cut (4-µm thick), mounted on silanized slides, and deparaffinized in xylol-alcohol. After routine histologic staining, each specimen's histologic diagnosis was made by two experienced ophthalmic pathologists.

RNA Isolation

Fifteen FFPE sections (4-µm thick) from each CNV membrane were collected and stored in tubes before RNA extraction. For the initial histopathologic evaluation, FFPE eyes of patients with ciliary body melanoma had been dissected by removing two scleral shells, leaving a central sclerocorneal ring segment. For the current study, the FFPE blocks were melted, and using a dissection microscope, the retina was carefully lifted off the RPE layer. Next, the RPE and choroid were cut laterally with a scalpel, and the central RPE/choroid complex, which easily detaches from the sclera in FFPE eyes, was retrieved and stored in low binding tubes until RNA extraction was performed. RNA isolation from FFPE specimens was performed as previously described.¹⁹ Briefly, total RNA was extracted from FFPE samples by using the Quick-RNA FFPE Kit (Zymo Research, Irvine, CA). Following DNase I digestion using the Baseline-ZERO Kit (Epicentre Technologies, Madison, WI), the RNA concentration was quantified by using the Qubit RNA HS Assay Kit on a Qubit Fluorometer (Thermo Fisher Scientific, Waltham, MA). RNA quality was determined via the RNA Pico Sensitivity Assay on a LabChip GXII Touch (PerkinElmer,

Waltham, MA). The fragment size of all RNA samples ranged between 120 and 150 bp.

MACE Libraries

The preparation of MACE libraries was performed by GenXPro GmbH (Frankfurt, Germany) using 1 µg of total RNA as previously described.¹⁹ Briefly, eight barcoded libraries (four CNV membranes and four RPE/choroidal control tissues) were sequenced simultaneously on the NextSeq 500 (Illumina, San Diego, CA) with 1 × 75 bp. The sequencing data reported in the current article have been deposited in the Gene Expression Omnibus database (<https://www.ncbi.nlm.nih.gov/geo>; accession number GSE146887).

Protein Analysis

Vitreous and plasma calprotectin levels were measured on vitreous and plasma samples from patients with nAMD undergoing vitrectomy for subretinal macular hemorrhage. Patients with macular pucker undergoing vitrectomy for epiretinal peeling served as control subjects. Frozen vitreous and plasma samples were thawed, and calprotectin levels were measured by using the Human S100A8/S100A9 Heterodimer Quantikine ELISA Kit according to the manufacturer's protocol (R&D Systems, Minneapolis, MN).

Immunohistochemistry

Human choroidal CNV membranes and control FFPE samples were cut into 5-µm sections and deparaffinized according to standard protocol. Sections were blocked with 5% normal goat serum in phosphate-buffered saline (PBS)/Triton-X 0.03% for 60 minutes at room temperature. Primary anti-S100 calcium-binding protein A9 (S100A9) antibody (sc-376772; Santa Cruz Biotechnology, Dallas, TX) was incubated in a 1:200 dilution in PBS containing 0.5% bovine serum albumin and

0.03% Triton-X overnight at 4°C. No primary antibody served as negative control. After extensive washing with PBS/Triton-X 0.03%, sections were incubated with an Alexa Fluor 647–labeled goat anti-mouse secondary antibody 1:500 in PBS/Triton-X 0.03% (Thermo Fisher Scientific) at room temperature for 1 hour in the dark. After washing at least three times with PBS/Triton-X 0.03% and Aqua Dest, auto-fluorescence was quenched with Sudan Black B (0.3% in 70% ethanol overnight, stirring at 50°C, filtrated twice, and incubated for 5 minutes at 37°C on the slides). Nuclei were counterstained with DAPI 1:10,000 for 5 minutes, washed three times with Aqua Dest, and mounted in Fluorescence Mounting Medium (Agilent Dako, Santa Clara, CA). Slides were imaged by using an Olympus BX-40 with a color camera (XM10, Olympus, Tokyo, Japan).

Statistics and Bioinformatics

Sequencing data were uploaded to and analyzed on the Galaxy web platform (usegalaxy.eu) as previously described.^{22,23} Quality control was performed with FastQC Galaxy version 0.72 (Barbraham Bioinformatics, Babraham, UK; <http://www.bioinformatics.babraham.ac.uk/projects/fastqc>, last accessed August 5, 2019). Reads were mapped to the human reference genome (hg38, Galaxy built-in reference genome) with RNA STAR Galaxy Version 2.6.0b-2²⁴ (default parameters) using the GENCODE annotation file (GENCODE 31, release June 2019, downloaded on August 5, 2019; <https://www.encodegenes.org/human/releases.html>).²⁵ Reads mapped to the human reference genome were counted by using featureCounts Galaxy Version 1.6.4²⁶ (default parameters) using the aforementioned annotation file.

The output of featureCounts was imported to RStudio version 1.2.1335 (R version 3.5.3). Gene symbols and gene types were determined based on Ensembl release 97 (July 2019) (Human genes, GRCh38.p12, downloaded on August 31, 2019).²⁷ Genes with 0 reads were removed from the analysis. Based on Ensembl gene types, genes were filtered for protein coding genes and small RNAs (long noncoding RNA, miRNA, miscellaneous RNA, small conditional RNA [scrRNA], small nucleolar RNA, snRNA, and small RNA). Genes coding for ribosomal or mitochondrial proteins were removed from the analysis. After principal component analysis, differential gene expression with Benjamini-Hochberg adjusted (adj.) *P* values was analyzed by using the R package DESeq2 version 1.22.2 (default parameters).²⁸

Transcripts with log₂fold change (log₂FC) >2 or <−2 and Benjamini-Hochberg adj. *P* < 0.05 were considered as differentially expressed genes (DEGs). Heatmaps were created with the R package ComplexHeatmap 1.20.0.²⁹ Data visualization with volcano plots was performed by using the ggplot2 package.³⁰ Gene enrichment analysis and its visualization with dotplots and cnetplots were performed by using the R package clusterProfiler 3.10.1.³¹ The 10 most significant Gene Ontology (GO) terms were visualized by using

dotplots. A cnetplot was used to illustrate the four most disease-associated GO terms and their associated DEGs.

To determine the cellular profile within the CNV micro-environment, the computational method xCell, which estimates the abundance scores of 64 immune and stromal cell types, including hematopoietic progenitors, epithelial cells, extracellular matrix (ECM) cells, and adaptive and innate immune cells, was applied.²⁰ Although the final xCell abundance scores cannot be directly interpreted as cell fractions, they showed high correlation with the true cell proportions.³² For xCell analysis, transcripts per million were calculated based on the output of featureCounts (assigned reads and feature length), as previously described.³³ Enrichment scores were compared between different groups by using *U*-tests. Cell types with *P* < 0.05 were considered to be significantly differentially enriched.

Results

Patient Characteristics

For MACE RNA-Seq analysis, four eyes of four consecutive patients with nAMD were included; four eyes of four patients with ciliary body melanoma requiring enucleation served as control samples. Three macroscopically normal eyes of three body donors served as control samples for immunohistochemical analysis. Patients' mean age was 79.5 years (range, 72 to 83 years) in the nAMD group, 73.0 years (range, 66 to 75 years) in the control group, and 82.7 years (range, 78 to 89 years) in the body donor group. CNV membranes were stored in paraffin for a mean of 7.264 days (range, 4346 to 7848 days) before RNA-Seq, and control samples were stored for 6.197 days (range, 3410 to 8057 days). Routine hematoxylin and eosin histology confirmed the diagnosis of CNV and revealed a microscopically intact retinal, RPE, and choroidal histology in the control and body donor samples (Figure 1). For protein quantification, seven consecutive patients with nAMD and 11 patients without AMD who underwent vitrectomy for subretinal bleeding or macular pucker were enrolled. The mean age of patients with nAMD was 77 years (range, 72 to 90 years); the mean age of the control patients was 70 years (range, 64 to 76 years). None of the patients exhibited concomitant macular disease, and only two patients with nAMD had received intravitreal bevacizumab injections 4 months before vitrectomy.

MACE RNA-Seq and Cell Type Enrichment Analysis in Human CNV

Using MACE RNA-Seq, a mean number of 907.233 reads (range, 297,004 to 1,744,933) in CNV samples and 4,889,361 reads (range, 348,446 to 11,898,565) in control samples were obtained. Because the RNA-Seq profile is a mixture of RNA from multiple cell types that include resident and infiltrating cells, bulk RNA cell type enrichment analysis was first used to recover the identity

of the cell types found in human CNV, using the gene signature expression–based cell type enrichment tool xCell.²⁰ Cell type enrichment scores across 64 immune and stromal cell types were obtained for both CNV and control specimens (Figure 2A and Supplemental Figure S1). These data show that immune scores were overall higher in CNV samples (0.025 ± 0.029) compared with the scores of healthy RPE/choroid samples (0.014 ± 0.013 ; $P = 0.27$). Among the different immune cell subpopulations, CD4 T-effector memory phenotype cells, CD4⁺ naive T cells, M1 macrophages, and natural killer T cells were significantly increased in CNV samples compared with levels observed in healthy control samples ($P < 0.05$) (Figure 2A). In contrast, T helper cells type 2 and basophils were significantly decreased in CNV samples compared with control samples. Of note, subpopulations of M2 macrophages were similar in CNV samples compared with control samples (Supplemental Figure S1). Overall stroma scores were significantly different between CNV samples (0.036 ± 0.036) compared with control samples (0.009 ± 0.008 ; $P < 0.05$). In particular, endothelial cells and microvascular endothelial cells were substantially increased in CNV samples compared with levels observed in healthy control samples ($P < 0.05$) (Figure 2A).

Differential Gene Expression in Human Choroidal Neovascularization

Of a total 29,334 different RNA transcripts, five differentially expressed transcripts that were decreased in CNV samples and 158 differentially expressed transcripts that were increased in CNV membranes compared with control samples (ie, $\log_2\text{FC} > 2$ or < -2 ; adj. $P < 0.05$) were determined. The top five differentially overexpressed transcripts in CNV membranes included the S100 calcium binding protein A8 (*S100A8*; $\log_2\text{FC} = 7.6$; adj. $P = 2.5 \times 10^{-5}$), *S100A9* ($\log_2\text{FC} = 7.0$; adj. $P = 1.5 \times 10^{-5}$), FKBP prolyl isomerase 8 (*FKBP8*; $\log_2\text{FC} = 7.3$; adj. $P = 3.5 \times 10^{-4}$), keratin 19 (*KRT19*; $\log_2\text{FC} = 7.2$; adj. $P = 1.4 \times 10^{-4}$), and vesicle-associated membrane protein 5 (*VAMP5*; $\log_2\text{FC} = 6.5$; adj. $P = 2.5 \times 10^{-3}$) (Figure 2B). The DEGs are provided (Supplemental Tables S1 and S2).

Enrichment Analysis of DEGs

To gain more insight into the biological pathways and molecular functions involved in human CNV formation, a GO cluster analysis was performed of the 158 DEGs that were up-regulated in the human CNV membranes. The DEGs contributed to biological processes, such as blood vessel development (GO:0001568; 29 counts; adj. $P = 1.7 \times 10^{-9}$), extracellular structure organization (GO:0043062; 26 counts; adj. $P = 4.7 \times 10^{-13}$), immune response–regulating signaling pathway (GO:0002764; 16 counts; adj. $P = 0.001$), and

response to wounding (GO:0009611; 21 counts; adj. $P = 1.8 \times 10^{-5}$) (Figure 2C and Supplemental Table S3). Molecular function (GO) enrichment analysis showed that the up-regulated genes were mainly involved in ECM structural constituent (GO:0005201; 14 counts; adj. $P = 1.5 \times 10^{-8}$), growth factor binding (GO:0019838; 12 counts; adj. $P = 3.3 \times 10^{-7}$), cell adhesion molecule binding (GO:0050839; 20 counts; adj. $P = 5.2 \times 10^{-7}$), integrin binding (GO:0043236; 7 counts; adj. $P = 0.003$), and cytoskeletal protein binding (GO:0008092; 23 counts; adj. $P = 1.1 \times 10^{-4}$) (Figure 2D and Supplemental Table S4). The top five prominent molecular mediators of the most disease-relevant biological processes enriched in human CNV are depicted (Figure 2E). Interestingly, *S100A8* and *S100A9* emerged as the most prominent DEGs in the immune-related cluster. All DEGs and CNV-associated genes enriched in the four most disease-relevant GO biological processes terms are illustrated in the cnetplot (Figure 3). As expected, a higher *VEGFA* (vascular endothelial growth factor A) expression level was also noted in human CNV membranes compared with control samples ($\log_2\text{FC} = 0.7$); the difference, however, was not statistically significant.

S100A8/A9 Expression in Human CNV

The RNA-Seq analysis revealed that both the *S100A8* (CNV, 42.98 reads; control, 0.05 reads; $\log_2\text{FC} = 7.6$; adj. $P = 2.5 \times 10^{-5}$) and *S100A9* (CNV, 166.36 reads; control, 1.41 reads; $\log_2\text{FC} = 7.0$; adj. $P = 1.5 \times 10^{-5}$), which together encode for the S100A8/A9 protein complex calprotectin, were significantly increased in human CNV compared with control tissue (Figure 4, A and B). To validate these findings on a protein level, S100A9 immunohistochemistry was performed on human CNV membranes and healthy control tissue. In line with the RNA-Seq results, only a weak S100A9 immunohistochemical staining was observed in the healthy eye, which was restricted to a few cells in the lumen of retinal vessels and in the interstitium of the choroid (Figure 4E). In human CNV membranes, in contrast, a plethora of S100A9-positive cells were found that exhibited phagocytic cups, indicating that these cells belong to the mononuclear phagocyte system (Figure 4F). Because S100A9 and S100A8 protein form a soluble and secreted heterodimer protein called calprotectin, a S100A8/A9 enzyme-linked immunosorbent assay of vitreous samples of patients with nAMD was then performed. The S100A8/A9 heterodimer was significantly increased in the vitreous of human patients with AMD (23.21 ± 10.05 ng/mL) compared with that of control subjects (3.89 ± 0.85 ng/mL; $P = 0.01$), strongly suggesting that S100A8/A9 accumulates in the vitreous during CNV formation (Figure 4C). Conversely, S100A8/A9 protein levels in the plasma of patients with nAMD (1311 ± 432.8 ng/mL) and control patients (1412 ± 394.8 ng/mL; $P = 0.79$) were not statistically significantly different (Figure 4D).

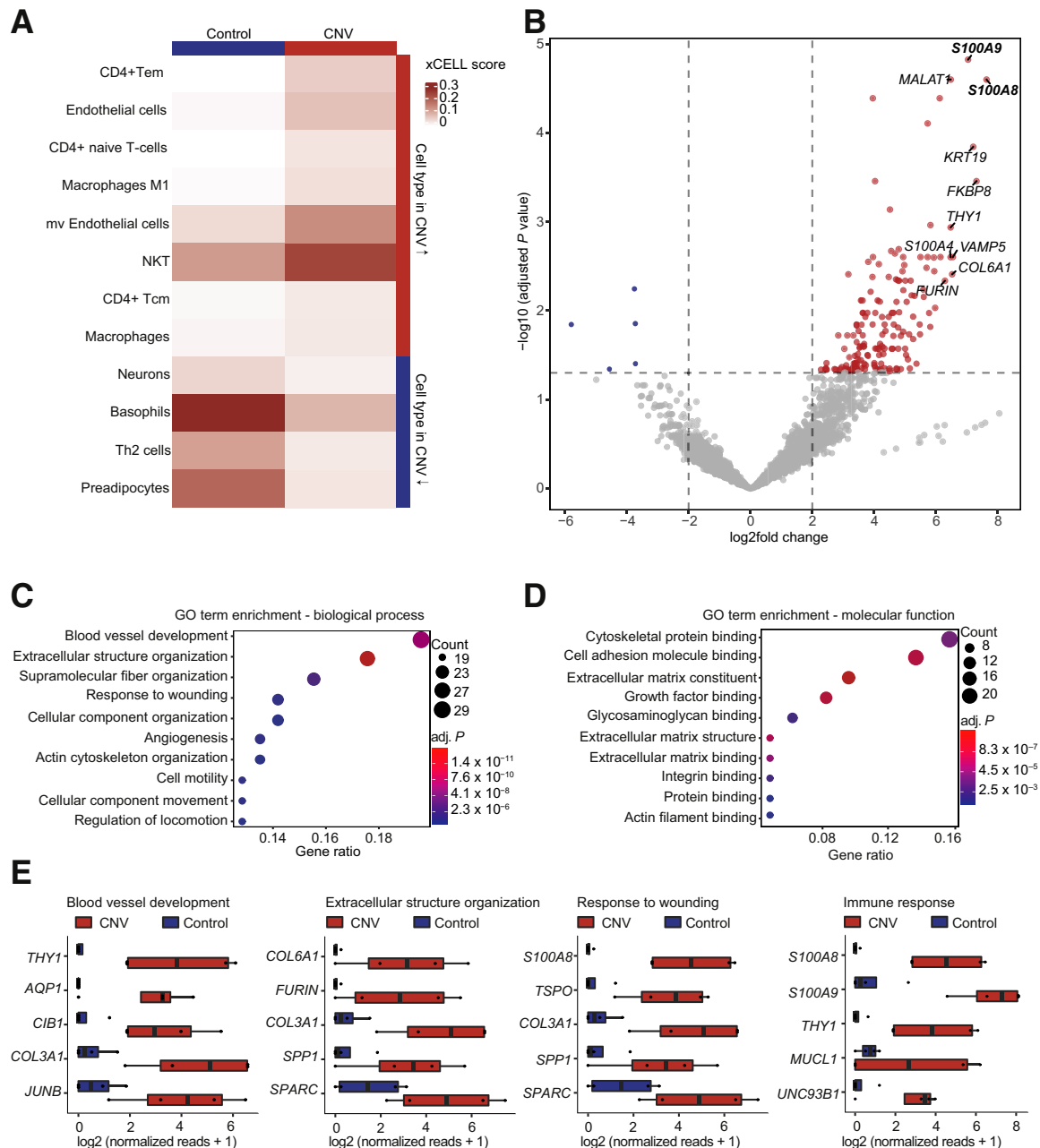


Figure 2 Cell type enrichment analysis of the RNA sequencing data and differentially expressed genes (DEGs) in human choroidal neovascularization (CNV) membranes compared with age-matched macular retinal pigment epithelium/choroidal tissue. **A:** Cell type enrichment analysis of the RNA sequencing data were determined by using xCell, a bioinformatics tool that generates cell type enrichment scores based on gene expression data for 64 immune and stromal cell types. The heatmap represents the mean enrichment score per group for 12 of the 64 cell types that were differentially enriched (U -test, $P < 0.05$) in human CNV versus control tissue. Eight of the 12 cell types are positively enriched, and four are negatively enriched in CNV versus control. **B:** Volcano plot depicting the up-regulated and down-regulated DEGs (red and blue dots, respectively) and genes not differentially expressed (gray dots) according to the \log_2 fold change and the adjusted (adj.) P value. The top 10 DEGs that are increased in CNV membranes are labeled. **C** and **D:** Gene Ontology (GO) enrichment analyses for the 158 DEGs significantly enriched in CNV membranes. Dot plot depicting the top 10 enriched GO terms for biological processes (**C**) and molecular function (**D**) ordered according to the number of DEGs associated with the GO term (count). The size of the dots represents the count, and the dots' colors represent the adj. P values. The gene ratio describes the ratio of the count to the number of all DEGs. **E:** Box plots illustrating the top five factors of the most disease-relevant GO terms ordered according to \log_2 fold change. CD, cluster of differentiation; NKT, natural killer T cell; Th2, T helper type 2.

Discussion

Deciphering the transcriptional changes and molecular and cellular mechanisms underpinning human CNV

formation is fundamental to understanding and effectively treating the disease. Advances in genomic technologies, such as microarrays, RNA-Seq, or whole genome methylation studies, enable important insights into the

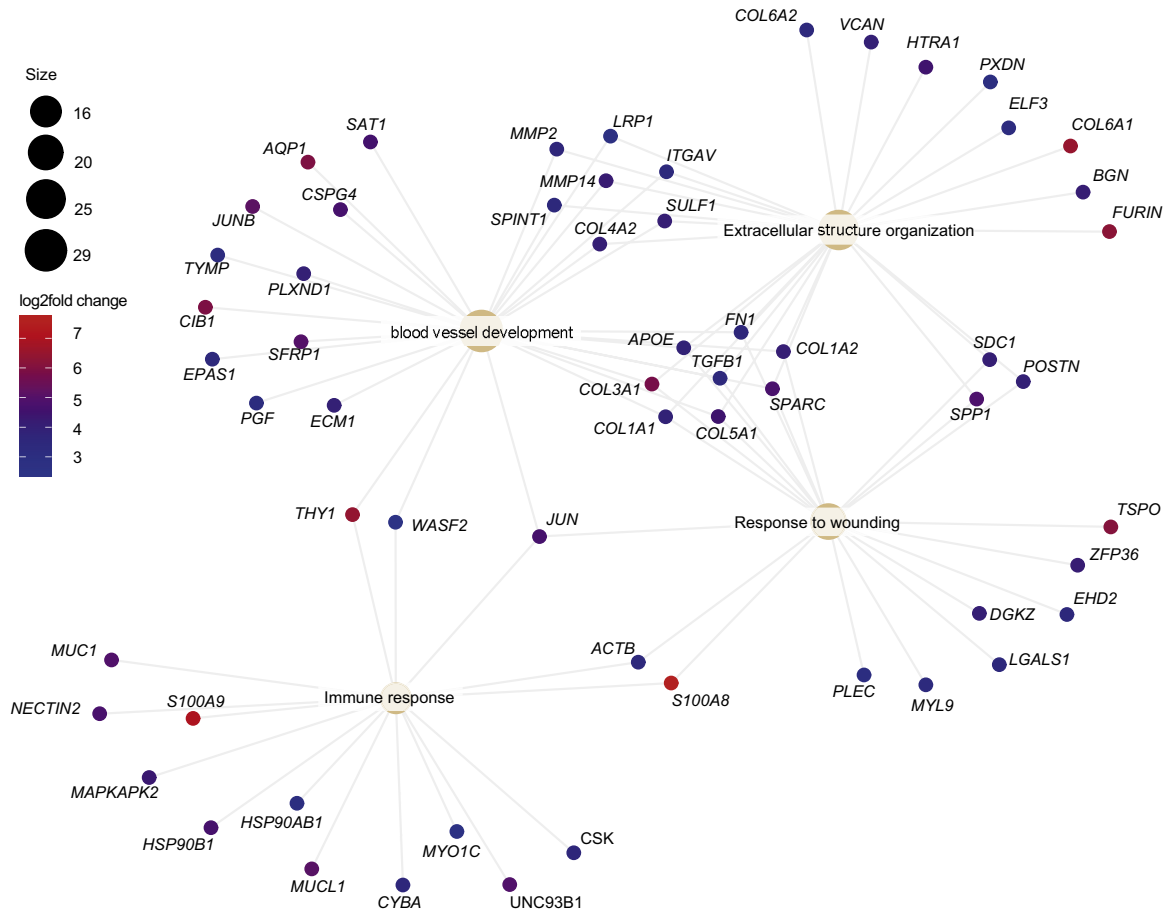


Figure 3 Gene Ontology (GO) enrichment analyses for the 158 differentially expressed genes disclose the potential molecular mediators underlying human choroidal neovascular membranes. The genes associated with the four most strongly disease-associated Gene Ontology biological processes terms are illustrated by the cnetplot, with the size of each node representing the number of overlapped genes in each term and color representing the log₂fold change of each differentially expressed gene.

transcriptional changes and pathways underlying CNV formation in patients with AMD.⁴ The current study is the first to exploit 3'-end RNA-Seq analysis of human CNV samples fixed in formalin immediately after surgical extraction, thus reducing the likelihood of bias by RNA degradation.

The comprehensive RNA-Seq analysis of human CNV membranes and healthy RPE/choroid revealed considerable differences in RNA expression levels and cellular composition between healthy and diseased tissue. A total of 158 differentially expressed transcripts were identified that were significantly increased in human CNV membranes compared with control tissue and are critical for three fundamental processes in CNV pathology: innate immune system responses, blood vessel development, and wound healing. The current study emphasizes the prevailing notion that activation of the innate immune system is associated with neovascular and scar-forming processes¹² and unravels novel molecular mediators underlying these processes, which have so far not been linked to nAMD. In agreement with the literature, the data suggest a critical role of proinflammatory M1 macrophages,^{34,35} T cells,^{36,37} and natural

killer T cells³⁸ in the pathogenesis of AMD and CNV, thus opening new perspectives for cell-specific treatment of immune-mediated conditions. In particular, evidence for a significant accumulation of CD4⁺ T memory cells was observed in CNV compared with the control samples. These results are consistent with other studies that found an increased number of T memory cells in the blood of patients with AMD compared with non-AMD control samples and suggest a 13.3-fold increased risk of developing AMD in patients with elevated blood levels of memory T cells and at least one CFH H402 risk allele.³⁶

Among the immunomodulatory CNV-associated processes, factors such as *TSPO*,³⁹ *LGALS* (galectin-1),⁴⁰ and *CXCL14*⁴¹ have already been linked to AMD. Others such as *C1r* or *PVRL2* (nectin-2) have not yet been associated with AMD and CNV formation, and they require further investigation. Additionally, several genes involved in blood vessel development were identified as being overexpressed in human CNV membranes, thus supporting previous reports.¹² Some of these genes, such as *APOE*,⁴² *Aquaporin 1*,⁴³ and *HIF2a* (*EPAS*),⁴⁴ have already been mentioned in the context of AMD and CNV formation, whereas others

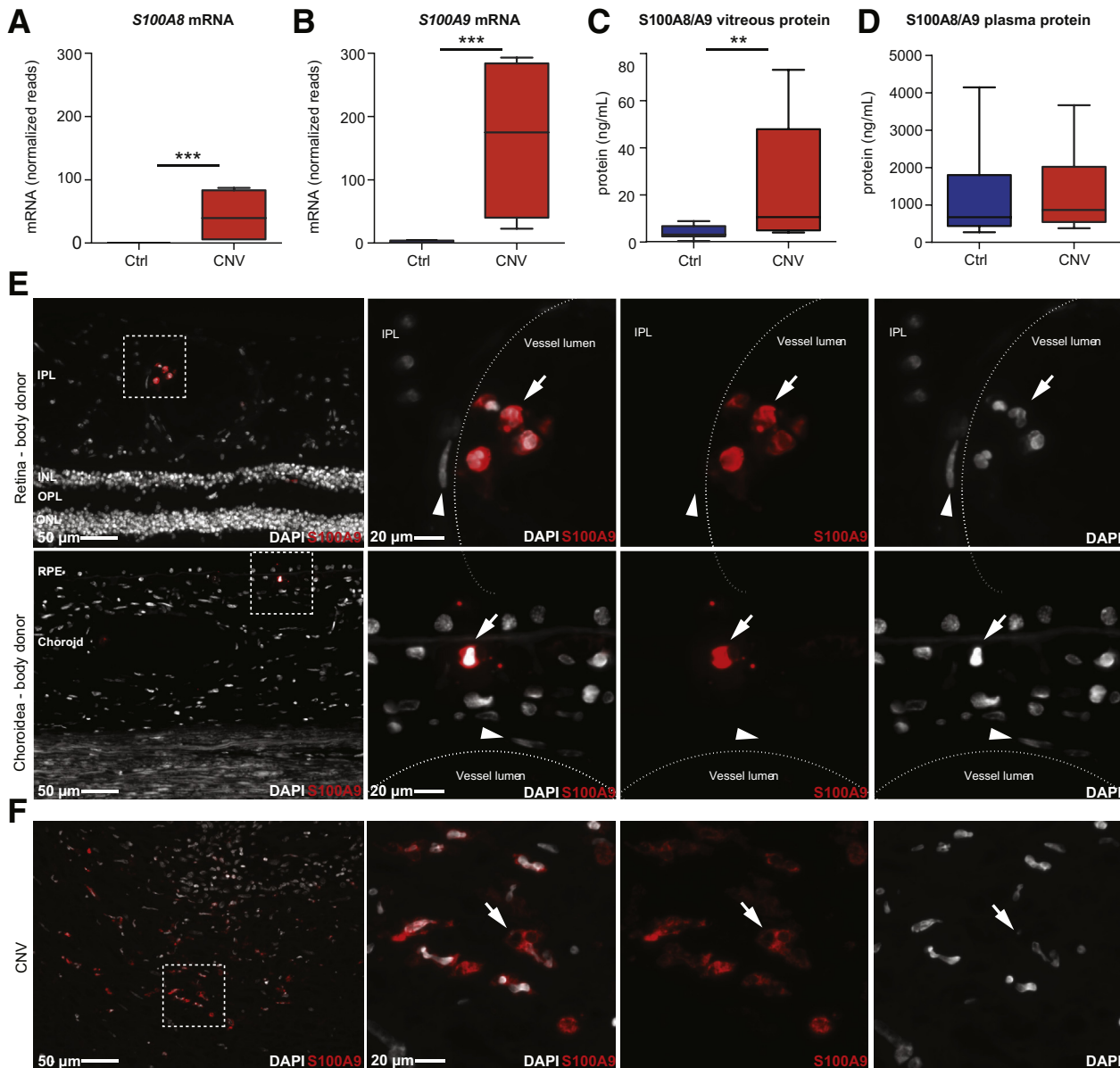


Figure 4 Expression of S100 calcium-binding proteins A8 and A9 (S100A8/A9) in human choroidal neovascularization (CNV) membranes compared with age-matched macular retinal pigment epithelium (RPE)/choroidal tissue. **A** and **B**: S100A8/A9 mRNA expression levels in CNV membranes compared with RPE/choroidal tissue measured by RNA sequencing (RNA-Seq). **C** and **D**: S100A8/A9 protein levels in the vitreous and plasma of patients with neovascular age-related macular degeneration and control (ctrl) subjects measured by using enzyme-linked immunosorbent assay (ctrl, $n = 11$; CNV, $n = 7$). **E** and **F**: Representative immunofluorescence images for S100A9 (red) and DAPI (white) in CNV membranes and age-matched RPE/choroidal ctrl tissue. **Boxed areas** are displayed in higher magnification to the right. **Arrows** in **E** indicate S100A9-positive cells in ctrl tissue (most likely granulocytes inside retinal vessels) and in human CNV membranes. **Dotted lines** represent vessel wall. **Arrowheads** indicate S100A9 negative pericytes. **Arrow** in **F** indicates a S100A9-positive cell displaying phagocytic cups. Data are expressed as means \pm SEM (*U*-test) (**C** and **D**). $n = 4$ control, CNV, and RPE/choroidal tissue (**A** and **B**); $n = 7$ CNV (**C** and **D**); $n = 11$ control (**C** and **D**). $**P < 0.01$, $***P < 0.001$. Scale bars: 50 μm (**E** and **F**, left column); 20 μm (**E** and **F**, middle and right columns). INL, inner nuclear layer; IPL, inner plexiform layer; ONL, outer nuclear layer; OPL, outer plexiform layer.

such as *SFRP1* (secreted frizzled related protein 1) have previously been associated with neurodegenerative brain disease.⁴⁵ The exact role of each of these factors and their potential as pharmaceutical targets for the treatment of CNV will need to be investigated in future studies.

Clinical studies and histologic analysis have shown that CNV membranes are often associated with excessive wound-healing responses, resulting in subretinal scarring.^{46,47} These

fibrotic processes are characterized by the proliferation and infiltration of various cell types such as RPE cells, glial cells, fibroblasts, and innate immune cells contributing to substantial remodeling of the ECM. In line with this hypothesis, this study detected many profibrotic and ECM-modulating factors, including *TGF- β 1* (transforming growth factor- β 1), *FNI* (fibronectin 1), and various collagen types, which are significantly increased in human CNV membranes. In

particular, TGF- β is involved in several aspects of subretinal fibrosis and can induce the expression of collagen-1 and fibronectin-1, two of the most prominent ECM components in the course of subretinal fibrosis,⁴⁸ underscoring the therapeutic potential of this target.⁴⁹ Other profibrotic factors such as *LGALS9* or *VCAN* (versican) that were increased in human CNV membranes in the current study have received less attention so far and might become future therapeutic targets.

In search of a soluble and secreted factor that could constitute an effective drug target, we identified *S100A9* among the top DEGs in human CNV membranes. Interestingly, *S100A9* was expressed in a plethora of phagocytic cells (most likely immune cells) in human CNV membranes, and that the *S100A8/A9* protein heterodimer was increased in the vitreous of human nAMD patients. *S100A8/A9* is constitutively expressed in myeloid cells such as granulocytes and macrophages, and it acts as a calcium sensor participating in cytoskeleton rearrangement and arachidonic acid metabolism under steady-state conditions. During inflammatory processes, *S100A8/A9* is increasingly expressed and actively secreted by myeloid cells to modulate the inflammatory response by stimulating leukocyte recruitment and cytokine secretion. *S100A8/A9* induces Toll-like receptor 4 or NF- κ B signaling and thereby the secretion of tumor necrosis factor- α , interleukin-1b, or interleukin-6, which can prolong and exacerbate inflammation.⁵⁰ Increased levels of *S100A8/A9* are a robust feature of aging and age-related inflammation in mammalian tissues, including the central nervous system, by activating receptors for advanced glycation end products, NF- κ B, and other signaling pathways.⁵¹ Of direct relevance to AMD, *S100* proteins are highly expressed in the macular region of human donor eyes⁵² and increased in the Bruch membrane and choroid complex in human donor eyes with AMD.⁵³ The current study results underline these findings and reveal *S100A8/A9* to be a candidate biomarker for diagnosis and follow-up of human nAMD, as well as a predictive indicator of therapeutic responses to inflammation-associated diseases. Because the pharmaceutical blockade of *S100A8/A9* activity reduces proinflammatory cytokine secretion and ameliorates excessive inflammation in human and murine disease, the heterodimer has potential as a therapeutic target.^{54–56}

This study is limited by its retrospective character and small sample size. Because the surgical approach entailing subretinal CNV extraction in patients with nAMD is now obsolete, a prospective study on human CNV membranes is not feasible. Furthermore, although the RPE and choroid of our control group were macroscopically and microscopically normal, the possibility that the expression profile in those tissues was altered due to the presence of a ciliary body melanoma at a distant site in the same eye cannot be fully excluded. However, because the macula was fundus-copically unaffected, and the RPE and choroid were microscopically normal, an effect from ciliary body

melanoma was considered to be unlikely. Another limitation of this study is that the bulk RNA-Seq approach used merely reflects the average gene expression of tissues and, in contrast to scRNA-Seq studies, cannot reveal important biological aspects of cell heterogeneity. However, scRNA-Seq on paraffin sections is not feasible. Instead, bulk RNA cell type enrichment analysis was used to recover the identity of the cell types found in human CNV. There are numerous methods currently available to assess heterogeneity in the tissue microenvironment. However, xCell is one of the most widely used and most robust tools based on the currently available data within the literature. Recently, a study systematically analyzed the capacity and limitations of multiple transcriptome-based cell-type quantification methods and reported that xCell exhibits correlation indexes for predicting macrophages and natural killer cells of 0.96 and 0.88, respectively, which is superior to those provided by other tools (eg, CIBERSORT).⁵⁷ It is important to note that the results of cell components were derived from *in silico* analysis; these results were not validated via histopathology because of the limited experimental conditions and sample acquisition difficulties. This limitation needs to be addressed in future studies. Finally, analysis from the current study revealed a considerable variability of number of reads, in particular within the CNV samples. However, because tissue processing and library preparation were kept standardized for all samples, it is assumed that the observed variability is explained by the given biological variability.

In conclusion, gene expression studies by MACE sequencing in human CNV membranes are feasible and provide an important initial step to determine the underlying cellular and molecular functions in nAMD. This study reveals novel biomarkers that are increased in human CNV membranes compared with healthy control tissue and that contribute to biological processes, including innate immune activation, ECM organization, and blood vessel development (Supplemental Figure S2). Among them, *S100A8/A9* has emerged as a promising biomarker for diagnosis and follow-up of human nAMD. The transcriptional differences described in this study provide new insights into the expression landscape of human CNV pathophysiology and reveal numerous targets for the development of AMD-directed diagnostics and pharmaceuticals.

Acknowledgments

We thank Gabriele Prinz, Marc Guder, Johannes Baumann, Constance Hobusch, and Matthias Oehme for excellent technical assistance.

Supplemental Data

Supplemental material for this article can be found at <http://doi.org/10.1016/j.ajpath.2020.04.004>.

References

- Wong WL, Su X, Li X, Cheung CMG, Klein R, Cheng CY, Wong TY: Global prevalence of age-related macular degeneration and disease burden projection for 2020 and 2040: a systematic review and meta-analysis. *Lancet Glob Health* 2014, 2:e106–e116
- Wecker T, Ehlken C, Bühler A, Lange C, Agostini H, Böhringer D, Stahl A: Five-year visual acuity outcomes and injection patterns in patients with pro-re-nata treatments for AMD, DME, RVO and myopic CNV. *Br J Ophthalmol* 2017, 101:353–359
- Maguire MG, Ying GS, Jaffe GJ, Toth CA, Daniel E, Grunwald J, Martin DF, Hagstrom SA; CATT Research Group: Single-nucleotide polymorphisms associated with age-related macular degeneration and lesion phenotypes in the comparison of age-related macular degeneration treatments trials. *JAMA Ophthalmol* 2016, 134:674–681
- Morgan DJ, DeAngelis MM: Differential gene expression in age-related macular degeneration. *Cold Spring Harb Perspect* 2014, 5:a017210
- Strunnikova NV, Maminishkis A, Barb JJ, Wang F, Zhi C, Sergeev Y, Chen W, Edwards AO, Stambolian D, Abecasis G, Swaroop A, Munson PJ, Miller SS: Transcriptome analysis and molecular signature of human retinal pigment epithelium. *Hum Mol Genet* 2010, 19:2468–2486
- Yoshida S, Yashar BM, Hiriyanna S, Swaroop A: Microarray analysis of gene expression in the aging human retina. *Invest Ophthalmol Vis Sci* 2002, 43:2554–2560
- Chowers I, Wong R, Dentchev T, Farkas RH, Iacovelli J, Gunatilaka TL, Medeiros NE, Presley JB, Campochiaro PA, Curcio CA, Dunaief JL, Zack DJ: The iron carrier transferrin is upregulated in retinas from patients with age-related macular degeneration. *Invest Ophthalmol Vis Sci* 2006, 47:2135–2140
- Liu F, Jansen TK, Trimarchi J, Punzo C, Cepko CL, Ohno-Machado L, Hovig E, Patrick Kuo W: Comparison of hybridization-based and sequencing-based gene expression technologies on biological replicates. *BMC Genomics* 2007, 8:153
- Ozsolak F, Milos PM: RNA sequencing: advances, challenges and opportunities. *Nat Rev Genet* 2011, 12:87–98
- Yendrek CR, Ainsworth EA, Thimmapuram J: The bench scientist's guide to statistical analysis of RNA-Seq data. *BMC Res Notes* 2012, 5:506
- Voigt AP, Mulfaul K, Mullin NK, Flamme-Wiese MJ, Giacalone JC, Stone EM, Tucker BA, Scheetz TE, Mullins RF: Single-cell transcriptomics of the human retinal pigment epithelium and choroid in health and macular degeneration. *Proc Natl Acad Sci U S A* 2019, 116:24100–24107
- Newman AM, Gallo NB, Hancox LS, Miller NJ, Radeke CM, Maloney MA, Cooper JB, Hageman GS, Anderson DH, Johnson LV, Radeke MJ: Systems-level analysis of age-related macular degeneration reveals global biomarkers and phenotype-specific functional networks. *Genome Med* 2012, 4:16
- Hunter A, Spechler PA, Cwanger A, Song Y, Zhang Z, Ying G, Hunter AK, deZoeten E, Dunaief JL: DNA methylation is associated with altered gene expression in AMD. *Invest Ophthalmol Vis Sci* 2012, 53:2089–2105
- Kim EJ, Grant GR, Bowman AS, Haider N, Gudiseva HV, Chavali VRM: Complete transcriptome profiling of normal and age-related macular degeneration eye tissues reveals dysregulation of anti-sense transcription. *Sci Rep* 2018, 8:3040
- Blair JA, Wang C, Hernandez D, Siedlak SL, Rodgers MS, Achar RK, Fahmy LM, Torres SL, Petersen RB, Zhu X, Casadesus G, Lee H: Individual case analysis of postmortem interval time on brain tissue preservation [Erratum appeared in *PLoS One* 2016;11:e0157209]. *PLoS One* 2016, 11:e0151615
- Wada T, Becskei A: Impact of methods on the measurement of mRNA turnover. *Int J Mol Sci* 2017, 18:2723
- Malik KJ, Chen CD, Olsen TW: Stability of RNA from the retina and retinal pigment epithelium in a porcine model simulating human eye bank conditions. *Invest Ophthalmol Vis Sci* 2003, 44:2730–2735
- Abdueva D, Wing M, Schaub B, Triche T, Davicioni E: Quantitative expression profiling in formalin-fixed paraffin-embedded samples by affymetrix microarrays. *J Mol Diagn* 2010, 12:409–417
- Lange CAK, Lehnert P, Boneva SK, Zhang P, Ludwig F, Boeker M, Hoffmeier K, Horres R, Schlunck G, Reinhard T, Böhringer D, Auw-Haedrich C: Increased expression of hypoxia-inducible factor-1 alpha and its impact on transcriptional changes and prognosis in malignant tumours of the ocular adnexa. *Eye (Lond)* 2018, 32:1772–1782
- Aran D, Hu Z, Butte AJ: xCell: digitally portraying the tissue cellular heterogeneity landscape. *Genome Biol* 2017, 18:220
- Bressler NM, Bressler SB, Hawkins BS, Marsh MJ, Sternberg P, Thomas MA; Submacular Surgery Trials Pilot Study Investigators: Submacular surgery trials randomized pilot trial of laser photocoagulation versus surgery for recurrent choroidal neovascularization secondary to age-related macular degeneration: I. Ophthalmic outcomes submacular surgery trials pilot study report number 1. *Am J Ophthalmol* 2000, 130:387–407
- Afgan E, Baker D, Batut B, van den Beek M, Bouvier D, Čech M, Chilton J, Clements D, Coraor N, Grüning BA, Guerler A, Hillman-Jackson J, Hiltmann S, Jalili V, Rasche H, Soranzo N, Goecks J, Taylor J, Nekrutenko A, Blankenberg D: The Galaxy platform for accessible, reproducible and collaborative biomedical analyses: 2018 update. *Nucleic Acids Res* 2018, 46:W537–W544
- Boeck M, Thien A, Wolf J, Hagemeyer N, Laich Y, Yusuf D, Backofen R, Zhang P, Boneva S, Stahl A, Hilgendorf I, Agostini H, Prinz M, Wieghofer P, Schlunck G, Schlecht A, Lange C: Temporo-spatial distribution and transcriptional profile of retinal microglia in the oxygen-induced retinopathy mouse model. *Glia* 2020, 68:1859–1873
- Dobin A, Davis CA, Schlesinger F, Drenkow J, Zaleski C, Jha S, Batut P, Chaisson M, Gingeras TR: STAR: ultrafast universal RNA-seq aligner. *Bioinformatics* 2013, 29:15–21
- Frankish A, Diekhans M, Ferreira A-M, Johnson R, Jungreis I, Loveland J: GENCODE reference annotation for the human and mouse genomes. *Nucleic Acids Res* 2019, 47:D766–D773
- Liao Y, Smyth GK, Shi W: featureCounts: an efficient general purpose program for assigning sequence reads to genomic features. *Bioinformatics* 2014, 30:923–930
- Zerbino DR, Achuthan P, Akanni W, Amode MR, Barrell D, Bhai J, et al: Ensembl 2018. *Nucleic Acids Res* 2018, 46:D754–D761
- Love MI, Huber W, Anders S: Moderated estimation of fold change and dispersion for RNA-seq data with DESeq2. *Genome Biol* 2014, 15:550
- Gu Z, Eils R, Schlesner M: Complex heatmaps reveal patterns and correlations in multidimensional genomic data. *Bioinformatics* 2016, 32:2847–2849
- Wickham H: *ggplot2: Elegant Graphics for Data Analysis*, ed 2. Basel, Switzerland: Springer International Publishing, 2016
- Yu G, Wang LG, Han Y, He QY: clusterProfiler: an R package for comparing biological themes among gene clusters. *OMICS* 2012, 16:284–287
- Finotello F, Trajanoski Z: Quantifying tumor-infiltrating immune cells from transcriptomics data. *Cancer Immunol Immunother* 2018, 67:1031–1040
- Wagner GP, Kin K, Lynch VJ: Measurement of mRNA abundance using RNA-seq data: RPKM measure is inconsistent among samples. *Theory Biosci* 2012, 131:281–285
- Cao X, Shen D, Patel MM, Tuo J, Johnson TM, Olsen TW, Chan CC: Macrophage polarization in the maculae of age-related macular degeneration: a pilot study. *Pathol Int* 2011, 61:528–535
- Cruz-Guilloty F, Saeed AM, Echegaray JJ, Duffort S, Ballmick A, Tan Y, Betancourt M, Viteri E, Ramkellawan GC, Ewald E, Feuer W, Huang D, Wen R, Hong L, Wang H, Laird JM, Sene A, Apte RS, Salomon RG, Hollyfield JG, Perez VL: Infiltration of proinflammatory M1 macrophages into the outer retina precedes damage in a mouse model of age-related macular degeneration. *Int J Inflamm* 2013, 2013:503725

36. Faber C, Singh A, Krüger Falk M, Juel HB, Sørensen TL, Nissen MH: Age-related macular degeneration is associated with increased proportion of CD56(+) T cells in peripheral blood. *Ophthalmology* 2013, 120:2310–2316
37. Camelo S: Potential sources and roles of adaptive immunity in age-related macular degeneration: shall we rename AMD into autoimmune macular disease? *Autoimmune Dis* 2014, 2014:532487
38. Hijioka K, Sonoda KH, Tsutsumi-Miyahara C, Fujimoto T, Oshima Y, Taniguchi M, Ishibashi T: Investigation of the role of CD1d-restricted invariant NKT cells in experimental choroidal neovascularization. *Biochem Biophys Res Commun* 2008, 374:38–43
39. Biswas L, Zhou X, Dhillon B, Graham A, Shu X: Retinal pigment epithelium cholesterol efflux mediated by the 18 kDa translocator protein, TSPO, a potential target for treating age-related macular degeneration. *Hum Mol Genet* 2017, 26:4327–4339
40. Wu D, Kanda A, Liu Y, Kase S, Noda K, Ishida S: Galectin-1 promotes choroidal neovascularization and subretinal fibrosis mediated via epithelial-mesenchymal transition. *FASEB J* 2019, 33:2498–2513
41. Sung HJ, Han JI, Lee JW, Uhm KB, Heo K: TCCR/WSX-1 is a novel angiogenic factor in age-related macular degeneration. *Mol Vis* 2012, 18:234–240
42. Levy O, Calippe B, Lavalette S, Hu SJ, Raoul W, Dominguez E, Housset M, Paques M, Sahel JA, Bemelmans AP, Combadiere C, Guillonnet X, Sennlaub F: Apolipoprotein E promotes subretinal mononuclear phagocyte survival and chronic inflammation in age-related macular degeneration. *EMBO Mol Med* 2015, 7:211–226
43. Tran TL, Bek T, la Cour M, Prause JU, Hamann S, Heegaard S: Aquaporin-1 expression in retinal pigment epithelial cells overlying retinal drusen. *Ophthalmic Res* 2016, 55:180–184
44. Sheridan CM, Rice D, Hiscott PS, Wong D, Kent DL: The presence of AC133-positive cells suggests a possible role of endothelial progenitor cells in the formation of choroidal neovascularization. *Invest Ophthalmol Vis Sci* 2006, 47:1642–1645
45. Esteve P, Rueda-Carrasco J, Inés Mateo M, Martín-Bermejo MJ, Draffin J, Pereyra G, Sandoñs Á, Crespo I, Moreno I, Aso E, Garcia-Esparcia P, Gomez-Tortosa E, Rábano A, Fortea J, Alcolea D, Lleo A, Heneka MT, Valpuesta JM, Esteban JA, Ferrer I, Domínguez M, Bovolenta P: Elevated levels of secreted-frizzled-related-protein 1 contribute to Alzheimer's disease pathogenesis. *Nat Neurosci* 2019, 22:1258–1268
46. Daniel E, Toth CA, Grunwald JE, Jaffe GJ, Martín DF, Fine SL, Huang J, Ying G, Hagstrom SA, Winter K, Maguire MG; Comparison of Age-related Macular Degeneration Treatments Trials Research Group: Risk of scar in the comparison of age-related macular degeneration treatments trials. *Ophthalmology* 2014, 121:656–666
47. Grossniklaus HE, Miskala PH, Green WR, Bressler SB, Hawkins BS, Toth C, Wilson DJ, Bressler NM: Histopathologic and ultrastructural features of surgically excised subfoveal choroidal neovascular lesions: submacular surgery trials report no. 7. *Arch Ophthalmol* 2005, 123:914–921
48. Das A, Puklin JE, Frank RN, Zhang NL: Ultrastructural immunocytochemistry of subretinal neovascular membranes in age-related macular degeneration. *Ophthalmology* 1992, 99:1368–1376
49. Zhang H, Liu ZL: Transforming growth factor- β neutralizing antibodies inhibit subretinal fibrosis in a mouse model. *Int J Ophthalmol* 2012, 5:307–311
50. Wang S, Song R, Wang Z, Jing Z, Wang S, Ma J: S100A8/A9 in inflammation. *Front Immunol* 2018, 9:1298
51. Swindell WR, Johnston A, Xing X, Little A, Robichaud P, Voorhees JJ, Fisher G, Gudjonsson JE: Robust shifts in S100a9 expression with aging: a novel mechanism for chronic inflammation. *Sci Rep* 2013, 3:1215
52. Skeie JM, Mahajan VB: Proteomic landscape of the human choroid-retinal pigment epithelial complex. *JAMA Ophthalmol* 2014, 132:1271–1281
53. Yuan X, Gu X, Crabb JS, Yue X, Shadrach K, Hollyfield JG, Crabb JW: Quantitative proteomics: comparison of the macular Bruch membrane/choroid complex from age-related macular degeneration and normal eyes. *Mol Cell Proteomics* 2010, 9:1031–1046
54. Björk P, Björk A, Vogl T, Stenström M, Liberg D, Olsson A, Roth J, Ivars F, Leanderson T: Identification of human S100A9 as a novel target for treatment of autoimmune disease via binding to quinoline-3-carboxamides. *PLoS Biol* 2009, 7:e97
55. Cesaro A, Anceriz N, Plante A, Pagé N, Tardif MR, Tessier PA: An inflammation loop orchestrated by S100A9 and calprotectin is critical for development of arthritis. *PLoS One* 2012, 7:e45478
56. Wang C, Klechikov AG, Gharibyan AL, Wärmländer SKTS, Jarvet J, Zhao L, Jia X, Shankar SK, Olofsson A, Brännström T, Mu Y, Gräslund A, Morozova-Roche LA: The role of pro-inflammatory S100A9 in Alzheimer's disease amyloid-neuroinflammatory cascade [Erratum appeared in *Acta Neuropathol* 2014;128:461]. *Acta Neuropathol* 2014, 127:507–522
57. Sturm G, Finotello F, Petitprez F, Zhang JD, Baumbach J, Fridman WH, List M, Aneichyk T: Comprehensive evaluation of transcriptome-based cell-type quantification methods for immunology. *Bioinformatics* 2019, 35:i436–i445